

APPENDIX

Land-use/land-cover composition of Apulia region

Overall, more than 82% of Apulia contains agro-ecosystems (Figure 1). The northern and somewhat the central part of the region include arable lands (39.8%) producing cereals and vegetables, while extensive century-old olive groves (22.6%), fruit orchards and vineyards (6.4%), and heterogeneous agricultural areas (13.3%) dominate the central and southern Apulia. Major towns and small urban settlements account only for 3.8% of the entire area. Natural habitats are unevenly distributed with major forested areas (7.3%) concentrated in the Gargano peninsula. Small remnants of xeric oak forests are interspersed with olive groves, shrub and herbaceous vegetation associations (1.4%) and permanent pastures (5.2%) in Dauno (northwest) and Murge Apennines (southwest).

Normalized Difference Vegetation Index (NDVI) from MODIS data

In their comprehensive study spanning the whole planet over the course of 18 years (1982-1999), Young and Harris (2005) demonstrate that vegetation changes indicated by NDVI are fairly consistent with significant published works (e.g. Walther et al. 2002; Parmesan and Yohe 2003) on recent environmental changes. To authenticate the sensitivity of NDVI to vegetation changes for the Apulia region, before it was used further for change detection, we used monthly NDVI averages for some land-cover categories in Apulia, based on random samples of 250 pixels for each land-cover, from MODIS 32-day composites with a 500-m pixel resolution (Barnes et al. 2003; NASA 2007). Data used span from January 2001 to January 2006, i.e. since when MODIS project started. We chose broad land-cover categories from the Corine land cover map, namely arable lands, permanent cultivations (mainly olive groves) and natural habitats like semi-arid herbaceous associations (mainly grasslands, garigue and steppes) and forests, differentiating among natural areas to appraise NDVI ability to indicate their annual trends and to choose the best timing for change detection (Figure A1).

As expected, NDVI averages showed rather distinct and characteristic seasonal inter-annual periodicities for each of the broad land-use/land-cover categories corroborating well-known vegetation changes in Apulia given by seasonal variations in climate and water regime as well agricultural practices. Mean NDVI paths of land-use/land-cover separate most of all during the hot and dry summers owing to drought most affecting semi-arid grasslands (e.g. in Murge), and to a lesser degree olive groves as they are moderately irrigated (Figure A1). Trends also highlight the strong vegetation activity of large natural forests in the Gargano National Park in summer, and agricultural practices like, e.g. sowing, growing, harvesting, and fire. Spurred on by these results on the sensitivity of NDVI to vegetation changes for Apulia, we proceeded further in using NDVI for change detection. Although MODIS imagery does not cover all the period of interest (1997-2001), we reasonably assumed the same NDVI trends occurred previously, and the period of middle-end of June of the late growing season was chosen for change detection (Figure A1).

Change detection is needed since inter-annual seasonal NDVI paths (Figure A1) reproduce average differences among land covers, but do not account for changes and/or gains or losses in each land-cover type.

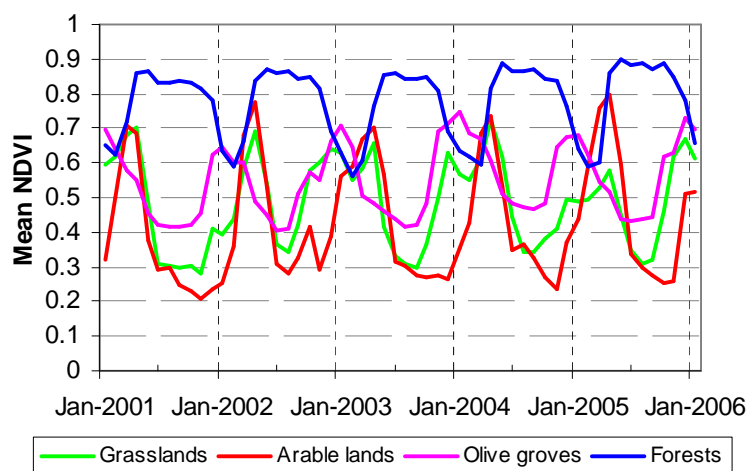


Fig. A1. NDVI monthly means from 2001 to 2006 for Apulia (South Italy) for four broad land-use/land-cover classes, as derived by MODIS imagery (Barnes et al. 2003), available only since the end of 2000. Trends are based on random samples of 250 pixels for each class. Standard errors are very small and are not shown.

Landsat image processing and change detection

Six cloud-free Landsat Thematic Mapper 5 (TM) and two Enhanced Thematic Mapper Plus (ETM+) images with a 30-m pixel resolution in the same period of vegetation phenological cycles at two different years, i.e. June 1997 and June 2001, have been processed to describe the pattern of change in Apulia (Table A1). For each of the six cloud-free Landsat Thematic Mapper 5 (TM) and two Enhanced Thematic Mapper Plus (ETM+) images registration is achieved by a first order polynomial function derived by a common set of a number of ground control points and a base map of the region. Inter-image spatial error given by the maximum root mean square error (RMSE) is about 9 m. Raw Landsat data are converted to at-satellite reflectance using header coefficients prior to atmospheric correction with a dark subtract procedure (Chavez 1988). The Landsat ETM+ NDVI image has been transformed to values matching the Landsat TM NDVI images using a linear transformation between images based on overlapping areas (with the lowest $r^2 = 0.97$). Finally, all NDVI scenes were mosaicked, and areas like lagoons, costal wetlands, seawater and small islands masked. Both single image composites showed quite distinct and similar NDVI values to those shown in Figure A1 for broad land covers.

Year		1997		2001	
Path	Row	Date (dd-mm, hh:mm)	Elevation (degree)	Date (dd-mm, hh:mm)	Elevation (degree)
189	31	15-06, 9:10*	60.78	26-06, 9:21*	62.06
188	31	24-06, 9:04*	60.58	27-06, 9:24 ⁺	63.39
	32	24-06, 9:04*	61.02	27-06, 9:24 ⁺	63.99
187	32	17-06, 8:58*	61.22	28-06, 9:09*	62.46

* Landsat TM 5; ⁺ Landsat ETM+ 7

Table A1. Characteristics of Landsat Thematic Mapper (TM) and Landsat Enhanced Thematic Mapper Plus (ETM+) images used for the change detection of Apulia (South Italy).

For change detection, a new raster image of the pixel-level NDVI standardized differences is derived for the entire region corresponding to the map of 4-year change intensity deviations from the mean intensity of change including both NDVI gains and losses (Zurlini et al. 2006). To capture real deviations, we define a threshold of change to obtain a binary (disturbed, undisturbed) map. This choice is arbitrary since more or less of the map will be classified as disturbed if a different threshold is used. For both real and simulated cases, we set the threshold corresponding to relatively extreme percentiles of 5% in both tails of the distribution (i.e. overall 10%, i.e., $P_d = 0.1$) of NDVI standardized differences. By doing so, we reduce the chance of analyzing either the pattern of “background noise” that could be obtained with much higher (e.g., 40%) percentiles, or of emphasizing few local extreme values (e.g., 1% or less).

Moving windows and disturbance trajectories for Apulia sub-regions (SELs)

Starting from the standardized change detection map (disturbance map) of Apulia, we “cut off” smaller maps corresponding to the geographic sub-regions of the first nested hierarchical level (i.e., provinces, Figure 1). We then proceed, within the first level, by “cutting off” further smaller geographic sub-sub-regions corresponding to the second nested hierarchical level (i.e., counties, Figure 1). Next, we use the moving window algorithm to measure the composition (P_d) and contagion (P_{dd}) of disturbance for pixels corresponding to the four land use classes (Table 1) and map the results.

We apply the moving window algorithm to the disturbance map, with ten window sizes, in pixel units, of 3x3, 5x5, 9x9, 15x15, 25x25, 45x45, 75x75, 115x115, 165x165, and 225x225, spanning from 0.81 to 4556.3 ha. Those window sizes are found to be suitably contained in all SEL surfaces in the panarchy after experimenting with different alternatives. To eliminate edge effects, we used only locations whose largest corresponding windows fit fully within the extent of each SEL, whereas for smaller SELs like counties we used also any location window fitting fully within the county area. We then derive, for each window size and nested sub-region, the average composition and contagion, to group locations over a range of window sizes according to land-use classes. Finally, we plot the resulting trajectories for each land use in the [P_d , P_{dd}] pattern state space along with the CP pertinent to each sub-region in the panarchy. Given the inherent spatial autocorrelation of composition and contagion, we derived estimates of standard error by randomly sampling 500 locations within each land use or cluster, both in real and simulated maps. Standard errors are very small and are not shown in the relevant figures.

Odds ratios

The odds ratio is defined here as the ratio of the odds of an event like total disturbed pixels over total undisturbed pixels which, for instance, make up one province, to the odds of the same event making up the SEL of reference like, e.g. the entire region. For example, suppose that, from change detection, 350 pixels are disturbed out of 1,000 making up one province nested in the region, so 650 pixels are undisturbed. In addition, suppose that 1,000 are disturbed out of 10,000 pixels making up the whole region. So 350/650 is the odds of a province getting disturbed pixels and for the region, it is 1,000/9,000. Calculating the odds ratio $(350/650) / (1,000/9,000) \approx 4.85$, the province results almost 4.85 times as likely to get disturbed pixels as the region. An odds ratio of 1 indicates that the event is equally likely in both SELs, while an odds ratio greater than 1 indicates that the event is more likely in the numerator SEL (e.g., province). Typically log-odds ratios are used taking the natural logarithm of the odds ratio which improves symmetry in large samples, so the sampling distribution of the log-odds ratio is roughly normal and the difference between the two proportions can be evaluated (Agresti

1996).

Generating neutral landscape patterns

We use the RULE software (Gardner 1999) to generate simulated random, multifractal and hierarchical landscape pattern maps of size 1024 x 1024 pixels, where P_d was fixed to 0.2 to get a congruous number of observations in the percentiles. In the multifractal model, the degree of spatial clumping is adjusted (RULE parameter H) to produce disturbances that are either relatively dispersed ($H = 0.1$) or aggregated ($H = 0.3$). For the hierarchical model, the RULE parameters describe the number of units (m_i) at each level i , and the fraction of disturbed units (p_i) at each level. We test one three-level map for which $(m_i, p_i) = (16, 0.5)$, $(8, 0.5)$, and $(8, 0.8)$ and one two-level map for which $(m_i, p_i) = (16, 0.8)$, $(4, 0.25)$ and $(16, 1.0)$ (Zurlini et al. 2007).

On each simulated map, P_d and P_{dd} are measured using the same ten window sizes used for real maps. As the clusters of P_d trajectories are similar to clusters of P_{dd} for the real landscapes (Zurlini et al. 2006), we incorporated information about the clumping of disturbance (P_{dd}) after the clusters are identified based on P_d values alone. To this end, we calculated the average P_{dd} value for all pixels contained within each cluster, for each window size. The clustering is performed using the ten P_d maps for each simulated map, with an unsupervised k -means algorithm (Legendre and Legendre 1998) as we did for clustering real locations (Figure 2). Recognizing that any clustering solution is at least partly arbitrary, we specify the identification of eight clusters to conform to the clustering solution adopted for real landscapes (Zurlini et al. 2006). By virtue of the coherent differential responses of eight clusters in the state space, we have confidence that the results are not spurious, but rather are informative about many interesting features of landscape pattern. The average P_d and P_{dd} values of the pixels in each of the eight clusters are then calculated at each of the ten window sizes providing a trajectory of each cluster at multiple scales in $[P_d, P_{dd}]$ space.

In particular, for simulated hierarchical maps, disturbance domains seem to describe local features (e.g., the edges of patches) and convergence is obtained because these local features are distributed more or less uniformly over the map (Zurlini et al. 2007). For those patterns, the average linear rate of increase of disturbance contagion across scales, for instance, of less disturbed clusters (C1 and C2) at three hierarchical levels (Figure A3, bottom), are very high ($\Delta P_{dd} \text{ km}^{-1}$ about 0.26) up to the rope where $P_{dd} = 0.58$. Hierarchical-like patterns are only found for certain sub-regions in Apulia with highly contrasting contagious source and sink areas (Zurlini et al. 2007).

For multifractal maps, disturbance domains also seem to describe local features like, e.g., the cores of patches which are distributed contagiously over the map so that convergence is obtained only asymptotically for the ideal window exactly equal to the entire geographic region. In this case, lag distances of disturbance contagion appear more or less equally distributed across scales, and the domains of disturbance seem to describe also convex and concave edges. Transitions to local patterns generally exhibit second-order stationarity on neutral model maps, except for hierarchical models, but not on real maps.

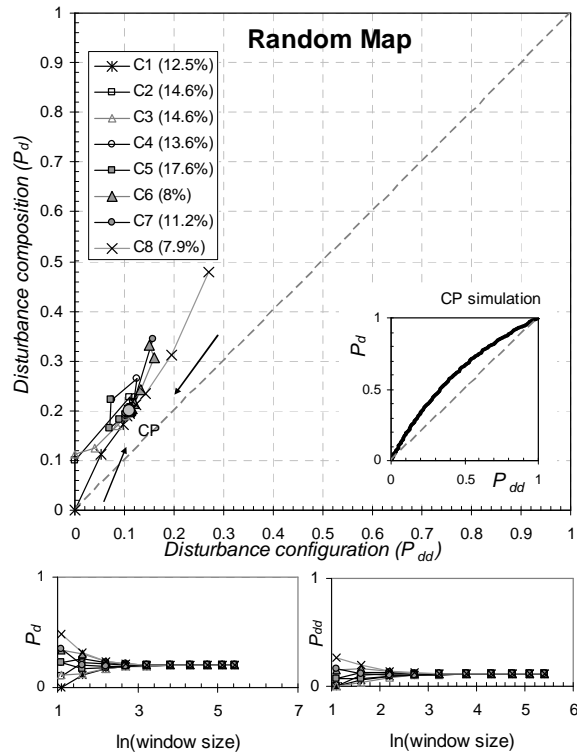


Fig. A2. Disturbance trajectories for eight clusters at multiple scales (ten window sizes) converging towards a regional convergence point (CP) and single trajectories of P_d and P_{dd} for random landscape patterns (adapted from Zurlini et al. 2007). The percentage of pixels belonging to each cluster is given in the legend (see text). The inserted figure shows the distribution of CP for 1.000 simulated random landscapes for disturbance ranging from zero (i.e., no disturbance) to 1 (i.e., fully disturbed).

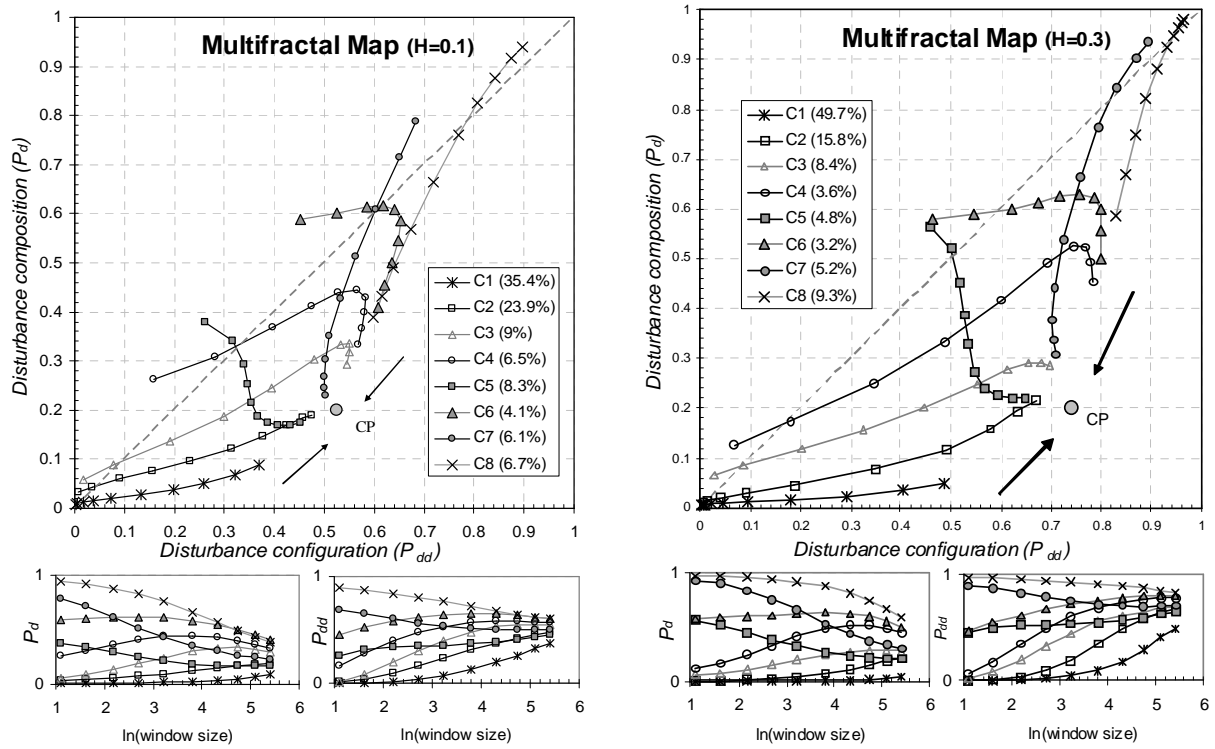


Fig. A3. Disturbance trajectories for eight clusters at multiple scales (ten window sizes) converging towards a regional convergence point (CP) for neutral multifractal landscape patterns (adapted from Zurlini et al. 2007). The percentage of pixels belonging to each cluster is given in the legend. Single trajectories of P_d and P_{dd} are given at the bottom of each neutral model.

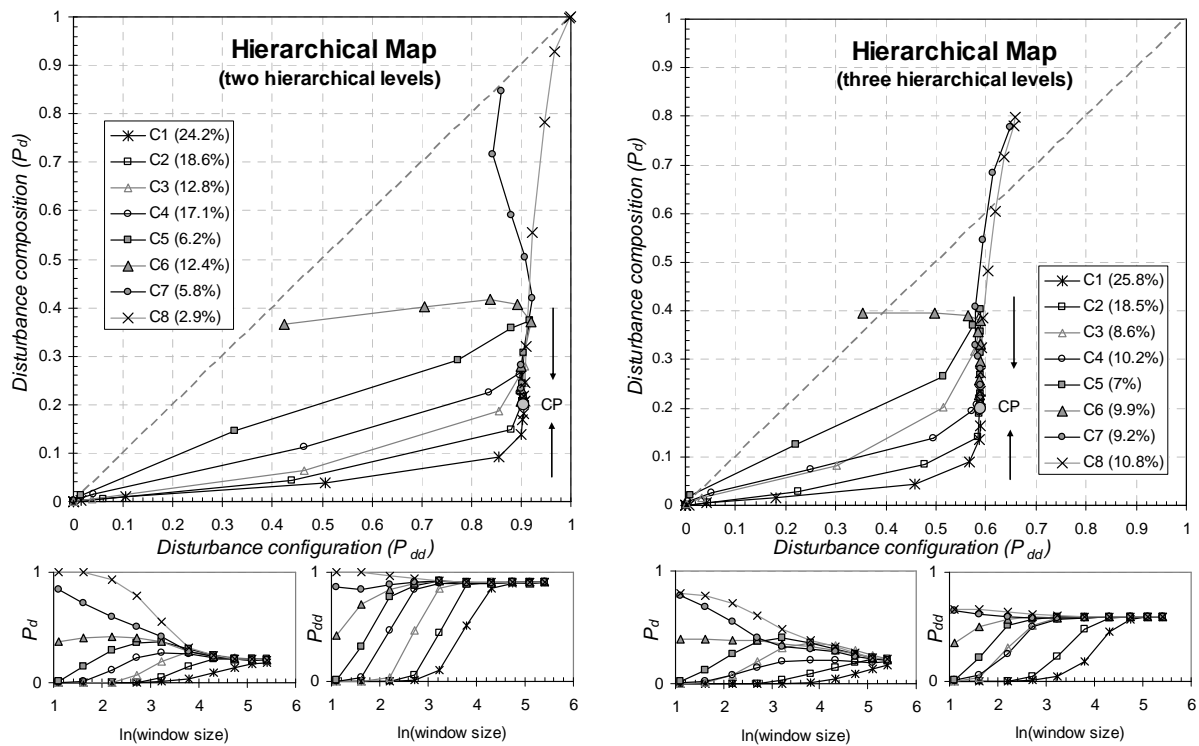


Fig. A4. Disturbance trajectories for eight clusters at multiple scales (ten window sizes) converging towards a regional convergence point (CP) for hierarchical landscape patterns (adapted from Zurlini et al. 2007). The percentage of pixels belonging to each cluster is given in the legend. Single trajectories of P_d and P_{dd} are given at the bottom of each neutral model.